Available online at www.sciencedirect.com
ScienceDirect
Trans. Nonferrous Met. Soc. China 34(2024) 2533−2551
Transactions of Nonferrous Metals Society of China
www.tnmsc.cn

Laser processing effects on Ti−45Nb alloy surface, corrosive and biocompatible properties

I. CVIJOVIĆ-ALAGIĆ[1], S. LAKETIĆ[1], M. MOMČILOVIĆ[1], J. CIGANOVIĆ[1], Đ. VELJOVIĆ[2], J. BAJAT[2], V. KOJIĆ[3], M. RAKIN[2]

1. Vinča Institute of Nuclear Sciences-National Institute of the Republic of Serbia, University of Belgrade, P.O. Box 522, 11001 Belgrade, Serbia;
2. Faculty of Technology and Metallurgy, University of Belgrade, Karnegijeva 4, 11120 Belgrade, Serbia;
3. Oncology Institute of Vojvodina, Faculty of Medicine, University of Novi Sad, Put Dr Goldmana 4, 21204 Sremska Kamenica, Serbia

Received 19 April 2023; accepted 20 October 2023

Abstract: The Ti−45Nb (wt.%) alloy properties were investigated in relation to its potential biomedical use. Laser surface modification was utilized to improve its performance in biological systems. As a result of the laser treatment, (Ti,Nb)O scale was formed and various morphological features appeared on the alloy surface. The electrochemical behavior of Ti−45Nb alloy in simulated body conditions was evaluated and showed that the alloy was highly resistant to corrosion deterioration regardless of additional laser surface modification treatment. Nevertheless, the improved corrosion resistance after laser treatment was evident (the corrosion current density of the alloy before laser irradiation was 2.84×10^{-8} A/cm^2, while that after laser treatment with 5 mJ was 0.65×10^{-8} A/cm^2) and ascribed to the rapid formation of a complex and passivating bi-modal surface oxide layer. Alloy cytotoxicity and effects of the Ti−45Nb alloy laser surface modification on the MRC-5 cell viability, morphology, and proliferation were also investigated. The Ti−45Nb alloy showed no cytotoxic effect. Moreover, cells showed improved viability and adherence to the alloy surface after the laser irradiation treatment. The highest average cell viability of 115.37% was attained for the alloy laser-irradiated with 15 mJ. Results showed that the laser surface modification can be successfully utilized to significantly improve alloy performance in a biological environment.

Key words: Ti−45Nb alloy; laser surface scanning; electrochemical properties; biocompatibility; cell morphology

1 Introduction

Biometallics have been extensively developed over the past decades as replacements for the non-functional skeleton parts of the human body [1,2]. Among all metallic biomaterials, titanium and its alloys are the most commonly used. To avoid failed implantation due to the release of toxic metal ions or the appearance of stress shielding effect, researchers developed a new class of titanium alloys that are free from elements with adverse health effects, such as Al and V, and elastic modulus closer to that of the human bone. These alloys are known as β-type Ti alloys [3−6]. The Ti−45Nb alloy (all alloy compositions in the present work are given in wt.%) is one of these alloys developed in recent years [3,7]. The presence of high Nb content in the alloy composition affects a relatively high alloy toughness and fatigue strength, low elastic modulus, and the appearance of more compact passivating surface layers which, in turn,

Corresponding author: I. CVIJOVIĆ-ALAGIĆ, Tel/Fax: +381-11-3408-224, E-mail: ivanac@vinca.rs
DOI: 10.1016/S1003-6326(24)66558-1

result in corrosion resistance improvement [2,8,9].

There are numerous compositions designed for the β-type Ti alloys that exhibit low elastic modulus and improved biocompatibility [3,4,7,9]. However, these are still unable to meet all implantation requirements primarily due to their non-active surface and limited corrosion resistance. Diverse surface modification methods are therefore proposed as treatments for the additional improvement of the corrosive and biological properties of the Ti alloys [10−12]. Laser surface scanning is one of these methods that can be employed to increase the surface roughness and bioactivity of these biometallics [13−16]. Advantages of this surface modification method are its rapid surface processing, ability to operate in different atmospheres and pressures, and possibility to modify only the selected surface areas. During the process of laser surface scanning, the laser beam irradiates the target material surface, inducing the formation of diverse melted layers [15,17]. The rate and direction of the melted layer solidification play an important role in the surface morphology formation processes and in great merit influence the properties and composition of surface layers formed during the irradiation [14,16,17]. Namely, the formation of diverse surface features (e.g. ripples and periodic wave-like) leads to an increase in the material surface roughness which, in turn, enables the protective surface layer to achieve higher adhesion and improved corrosion resistance.

One of the most important requirements for the metallic biomaterial surgical application is its high corrosion resistance [18−22]. Namely, when the biometallic is in contact with an electrolytic medium, the metallic surface becomes susceptible to corrosion, which induces a deterioration of the material and its properties. The presence of a thin Ti-oxide film on the biometallics surface is favorable to their damage resistance because it protects the material from further oxidation, and in that way enhances its corrosion performance and biocompatible properties [23−27]. Hence, the surface oxide film properties in great merit influence the electrochemical behavior of the metallic materials in biological environments and cell adhesion to their surfaces [28,29]. Some studies showed that the enhancement of surface layer properties can be achieved with an appropriate surface treatment, suggesting its positive effect on the alloy biomechanical behavior [30−32]. For example, YUE et al [30] showed that significant improvement in corrosion resistance of the Ti−6Al−4V alloy was obtained when the alloy surface was subjected to the laser treatment in nitrogen or argon atmosphere.

The implant surface characteristics are also very important for implant−tissue interactions [33]. Two essential aspects of these interactions are bioactivity and biointegration. Namely, the cell and tissue responses are affected not only by the chemical composition of the material surface but also by the implant surface topography and roughness [33−36]. Hence, there is also a need to enhance the surface roughness of implant materials through surface modification treatments [37,38]. Several research groups investigated the modification of materials' surface biocompatibility by applying laser irradiation [39−43]. They reported that the laser surface modification enhanced the cell's response and interaction with the substrate surface. Results of their studies showed that adhesion and proliferation of the pre-osteoblast cells were enhanced in the case of laser-scanned substrate compared to the as-received alloy. Similarly, DOU et al [44] investigated the influence of laser scanning on the morphological and wetting properties of the Ti alloy surface and showed that laser scanning caused the formation of stable hydrophilic surface suitable for the material biointegration. Furthermore, XU et al [45] showed that the scanning speed significantly affected the resulting surface roughness, while research results of the WANG et al [46] revealed that the promotion of TiO_2 formation and the oxide layer thickness increase on the laser-modified alloy surface is caused by the attainment of high temperature during the laser ablation treatment. Moreover, KEDIA et al [47] indicated that the usage of laser surface texturing and the formation of micro-groove patterns result in better cell adhesion, alignment, and spreading, and, in that way, improve material biological function.

Therefore, the main goal of the present study was to examine the laser surface scanning method as a suitable technique for the improvement of β-type Ti alloy surface bioactivity that will ensure the good adhesion of fibroblast cell cultures, as well as their rapid and continuous growth and proliferation. Having that in mind, laser irradiation

was utilized to modify the chemical composition and topography of the alloy surface to obtain the specific surface morphology complimented with an external oxide layer that could facilitate the alloy interaction with biological systems and, at the same time, protect the biometallic from further corrosion degradation.

2 Experimental

2.1 Material processing

Material used in the present study was the Ti−45Nb alloy supplied by ATI Specialty Alloys and Components, AL, USA, with the chemical composition reported in the previous work [48]. The alloy was received as a hot-extruded bar with 50 mm in diameter. The test samples were cut in the form of disks with 7 mm in thickness and 10 mm in diameter and mechanically ground using the SiC grinding papers up to 1000-grit and cleaned with ethanol in an ultrasonic bath.

The laser surface scanning was conducted in air to modify the Ti−45Nb alloy surface properties. For that purpose the Nd:YAG system EKSPLA SL 212/SH/FH operated at a wavelength of 1064 nm in the fundamental transverse TEM_{00} mode was utilized. The radiation scan speed was 0.3 mm/s and the laser pulse repetition rate was 10 Hz. To determine the influence of laser irradiation parameters on the alloy surface morphology and roughness, two different laser output energies, i.e. 5 and 15 mJ, were used. During the experiment, the pulse energy densities were maintained at 0.13 and 0.38 J/cm^2 for the laser output energies of 5 and 15 mJ, respectively. Irradiation was conducted by focusing the laser beam on the alloy surface with a quartz lens of 15.2 cm focal length and surface profiles were obtained in localized 1.092 mm × 1.092 mm area. The laser beam incidence angle to the sample surface was 90°.

2.2 Microstructure and surface characterization

The microstructure of as-received hot-extruded Ti−45Nb alloy was investigated in the extrusion direction by the electron backscatter diffractometer (EBSD) coupled with a Zeiss Leo 1525 scanning electron microscope (SEM). To identify the compounds and phases formed in the laser-affected surface area, the X-ray diffractometry (XRD) was utilized and for that purpose a Rigaku Ultima IV diffractometer with nickel filtered Cu K_α incident radiation and 1.541 Å wavelength was used at 40 kV voltage and 40 mA current. The scan was set in a 2θ angle range from 20° to 100° with a step size and scanning speed of 0.02° and 2 (°)/min, respectively. The Ti−45Nb alloy morphology after laser scanning was analyzed by a field-emission scanning electron microscope (FE-SEM) TESCAN Mira3 XMU operated at 20 kV. The variation of the surface composition with the laser irradiation parameters, such as laser output energy, was investigated in triplicate with excellent reproducibility by using a energy dispersive spectrometer (EDS) Oxford Inca 3.2 coupled with a SEM JEOL JSM 5800 operated at 20 kV and the obtained results were presented with calculated standard deviation (SD). Additionally, the morphological features of the alloy surface were characterized by using a non-contact optical profilometer ZYGO NewView 7100 with the 3D surface topographic and surface roughness measurements.

2.3 Electrochemical testing

The potentiodynamic polarization analysis and the electrochemical impedance spectroscopic (EIS) measurements were used to analyze the electrochemical behavior of the Ti−45Nb alloy before and after the laser surface scanning in the simulated human body conditions. Measurements were performed at (37±0.1) °C using a three-electrode cell configuration. The Ringer's solution with pH of 6.8, composed of 6.8 g/L NaCl, 0.4 g/L KCl, 0.2 g/L $CaCl_2$, 0.2048 g/L $MgSO_4·7H_2O$, 0.1438 g/L $NaH_2PO_4·H_2O$, 1.1 g/L $NaHCO_3$, and 1 g/L glucose, served as an electrolyte during testing, as a simulated body fluid (SBF). In a three-electrode cell configuration the alloy sample was a working electrode, the platinum grid was used as a counter electrode, while the saturated calomel electrode (SCE) was a reference electrode. Electrochemical measurements were performed using a Gamry Reference 600 Potentiostat/ Galvanostat/ZRA placed in the Faraday cage. Prior to the electrochemical measurements, the alloy samples were immersed in the electrolyte and allowed to stabilize at the open circuit potential (OCP). Linear polarization measurements were performed in the potential range from −0.75 to

4 V (vs SCE) with 1 mV/s scan rate. The EIS measurements were conducted at OCP using a sinusoidal signal with 10 mV amplitude and frequencies in the range of 0.01 Hz−100 kHz, as reported previously [48]. The recorded EIS data was analyzed using the Gamry Instruments Echem Analyst v.5.50 software.

2.4 Biocompatibility assessment

2.4.1 Cytotoxicity testing

The cytotoxicity of the Ti−45Nb alloy was assessed by two types of in vitro tests: colorimetric methyl-thiazol-tetrazolium (MTT) and tryptan blue exclusion (DET). The evaluation of the alloy cytotoxicity before and after the laser surface scanning was performed using the human fibroblast MRC-5 cell line (Human fibroblast, American Type Culture Collection CCL 171) following the procedure already described in the literature [49]. The cells were grown in flasks (Costar, 25 cm^2) in Dulbecco's modified Eagle's medium (DMEM) with 4.5% of glucose, 10% of fetal calf serum (FCS), and antibiotic antimycotic solution supplied by Sigma-Aldrich, USA. The cells were sub-cultured twice a week and a single cell suspension was obtained using 0.25% trypsin or trypsin in EDTA (Serva). The cell lines were cultured at 37 °C in 5% CO_2 air atmosphere with 100% humidity. Exponentially grown cells were used for investigation purposes. The cell density and viability were attained using the color rejection test with 0.1% trypsin blue showing that the viability of cells used in the assay was higher than 90%. All alloy test samples were sterilized and placed in Petri dishes with 50 mm × 9 mm in size (Falcon) with viable cells seeded on the alloy sample surface in the concentration of 2×10^5 mL^{-1}. The control samples contained only cells. The Petri dishes that contained the investigated alloy samples and seeded cells were thermostated for 48 h at 37 °C in humidified 5% CO_2 air atmosphere, and after the expiration of this incubation period, the cells were separated from the alloy samples utilizing the trypsinization treatment by adding 0.5% trypsin solution. The cytotoxicity of the Ti−45Nb alloy was determined as a percentage of the cell growth inhibition by conducting DET and MTT tests. During the DET testing the cell viability and number were evaluated using a trypan blue exclusion method and the cells' inhibition of growth (CI), i.e. cytotoxicity, was given in percentage according to the formula: $CI=N_s/N_k\times100\%$, where N_k is the average number of the cells in the control samples, while N_s is the average number of the cells in the samples containing the investigated Ti−45Nb alloy. Growth inhibition was also evaluated by tetrazolium colorimetric MTT assay (Sigma). The assay is based on the cleavage of the tetrazolium salt MTT, i.e. 3-(4,5-dimethylthiazol-2-yl)-2,5-diphenyl tetrazolium bromide, to formazan by mitochondrial dehydrogenases in viable cells. For the MTT testing, the exponentially growing cells were harvested, counted by trypan blue exclusion test, and plated into 96-well microtiter plates (Costar) at an optimal seeding density of 5×10^3 cells/well to assure a logarithmic growth rate throughout the assay period. Viable cells were planted at a volume of 100 μL/well in a complete medium at 37 °C for 48 h. 10 μL of the MTT solution was added to all wells 3 h before the end of the incubation period. MTT was dissolved in a medium at 5 mg/mL and filtered to sterilize and remove a small amount of insoluble residue present in some MTT batches. Cells were incubated in the presence of MTT for 3 h at 37 °C followed by the medium and MTT removal by suction. The formazan product was then solubilized in 100 μL of 0.04 mol/L HCl in isopropanol. After a few minutes, the optical density (OD) was read at room temperature on the Multiscan MCC340 spectrophotometer plate reader (Labsystems) at the wavelength of 540 nm and the reference wavelength of 690 nm. The wells without cells that contained only medium and MTT acted as blank. The cells' inhibition of growth CI was presented in percentages according to the formula: $CI=(OD_s/OD_k)\times100\%$, where OD_k is the average absorbance of the control samples, while OD_s is the average absorbance of the samples containing the investigated Ti−45Nb alloy. The in vitro tests were conducted in triplicate to confirm the results reproducibility.

2.4.2 Morphology analysis of live cells

Morphological features of the MRC-5 cells grown in contact with the investigated Ti−45Nb alloy samples were examined using an FE-SEM TESCAN Mira3 XMU microscope operated at an accelerating voltage of 20 keV. For that purpose, the MRC-5 cells were collected during the logarithmic phase of growth, trypsinized, resuspended, counted

in 0.1% trypan blue, seeded directly on the alloy samples surfaces in the concentration of 1.0×10^5 cells/mL, and cultivated at 37 °C in 5% CO_2 humidified atmosphere for 48 h. When the incubation period was over, the MRC-5 cells were fixed in 2.5% glutaraldehyde (Sigma) for 48 h, and then dehydrated in the four-step process using 3% acetic acid, 3% acetic acid and 25% ethanol solution with 1:1 volume ratio, 3% acetic acid and 50% ethanol solution with 1:1 volume ratio, and 70% ethanol. Finally, using a Baltec SCD 005 sputter coater, the Ti−45Nb alloy samples with fixed and dehydrated MRC-5 cells were coated with a thin Au film before their FE-SEM analysis.

3 Results and discussion

3.1 Microstructural characteristics

Results of the EBSD microstructural analysis of the hot-extruded Ti−45Nb alloy in the initial state, presented in Fig. 1(a), showed an equiaxed microstructure and pronounced recrystallized texture, which is in accordance with previously reported data available in the literature [50]. The XRD analysis (Fig. 1(b)) and previously reported results of the theoretical structural investigations on ab initio level [51] revealed the presence of two phases, i.e. body-centred cubic (bcc) β-Ti and orthorhombic Ti4Nb, in the as-received alloy microstructure.

After laser irradiation, the modified alloy was additionally analyzed by the XRD method and recorded XRD patterns showed that there was no phase transformation during the laser treatment even though the alloy surface exhibited morphological features typical for rapid melting and solidification (Fig. 1(b)). Namely, the XRD peaks that corresponded to the β-Ti and Ti4Nb phases are visible before and after the irradiation. Diffraction peaks observed at 2θ values of ~38.5° and 82° can be associated with (110) and (220) reflections of the bcc β-Ti phase with *Im*3*m* space group, respectively. The peak present at 39.1° belongs to the (111) reflection of the Ti4Nb orthorhombic phase with the *Cmcm* space group.

However, the XRD analysis of the laser-treated surfaces revealed the presence of diffraction peaks at 36.1° and 39.5° that correspond to the (Ti,Nb)O oxides (Fig. 1(b)). This suggests that the Ti−45Nb alloy surface was oxidized during the laser irradiation in the air atmosphere. Moreover, according to the observed XRD peak intensities it is evident that the oxidation level increased with an increase in the laser pulse energy and the formation of a thicker surface oxide layer occurred.

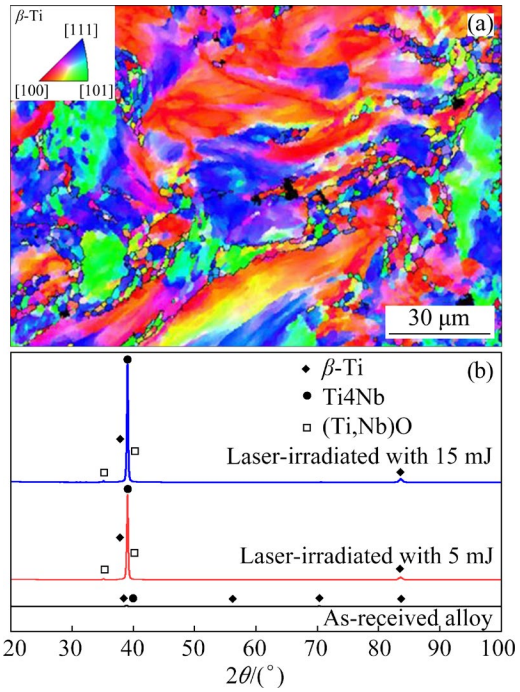

Fig. 1 Inverse pole figure map of as-received Ti−45Nb alloy (a), and XRD patterns of Ti−45Nb alloy in as-received and laser-treated conditions

3.2 Surface characteristics

The laser irradiation energy distribution during the alloy laser surface irradiation treatment plays an important role in the surface morphological modifications that can be achieved [13,15−17]. The part of the irradiation energy that is absorbed by the surface layer influences the rates of alloy surface heating, melting, cooling, and solidification. By varying irradiation parameters, such as laser pulse energy, scanning speed, scanning direction, focal position, wavelength, spot size, and surrounding atmosphere, it is possible to achieve the formation of specific surface morphology suitable for the improvement of alloy surface roughness, as well as its corrosive performance. Therefore, the laser-induced surface damage characteristics are mostly determined by irradiation parameters, i.e. laser pulse energy and scanning speed, which also influence the resulting ablation effect [14,17].

In the present study, the application of laser surface scanning method resulted in distinctive

surface morphological changes. Namely, the material heating and melting in the alloy surface and subsurface zone caused a part of the material to be removed as a result of the laser ablation process. Due to the rapid cooling after the laser beam action was completed, the melted material was quickly solidified, and distinctive surface damage features appeared in the form of diverse peaks and valleys, while the melted material accumulation led to the formation of periodic wave-like structures in the form of ripples (Fig. 2).

FE-SEM micrographs given in Fig. 2 also show that the application of laser pulse energy of 5 mJ led to the appearance of discrete unidirectional scan lines in the form of ripple-like structures and microcracks on the alloy surface (Fig. 2(b)). When the irradiation energy was increased, the periodic ripple-like structures gradually spread over the surface and exhibited a uniform periodicity (Fig. 2(c)). Moreover, most of the formed periodic structures were aligned parallel to the scanning direction, while the formed microcracks were more pronounced.

Additionally, the alloy surface profilometric analysis before and after irradiation showed that after the laser scanning was completed, distinctive surface morphological alterations were generated (Fig. 3). Such alterations are indicative of the rapid solidification process. As shown in Figs. 3(a, c, e), various degrees of rapid material solidification, induced by different laser pulse energies, resulted in the diverse range of periodic wave-like structures generated on the material surface determining the resulting surface topography in that way. The wave-like and ripple-like structures were defined according to the scanning direction (Figs. 3(c−f)). With an increase in the laser pulse energy, more pronounced hydrodynamic effects in the form of wave-like structures with some solidified ripples formed in the irradiated zone due to the attainment of high temperature and the laser beam intensity redistribution (Figs. 3(e, f)). This is in accordance with the results presented in the study of LI et al [52], where it was demonstrated that laser-treated surface morphology was mostly consistent with the laser scanning patterns.

By varying the laser operational parameters, it was also possible to vary the material surface roughness (Fig. 3). Namely, with an increase in the

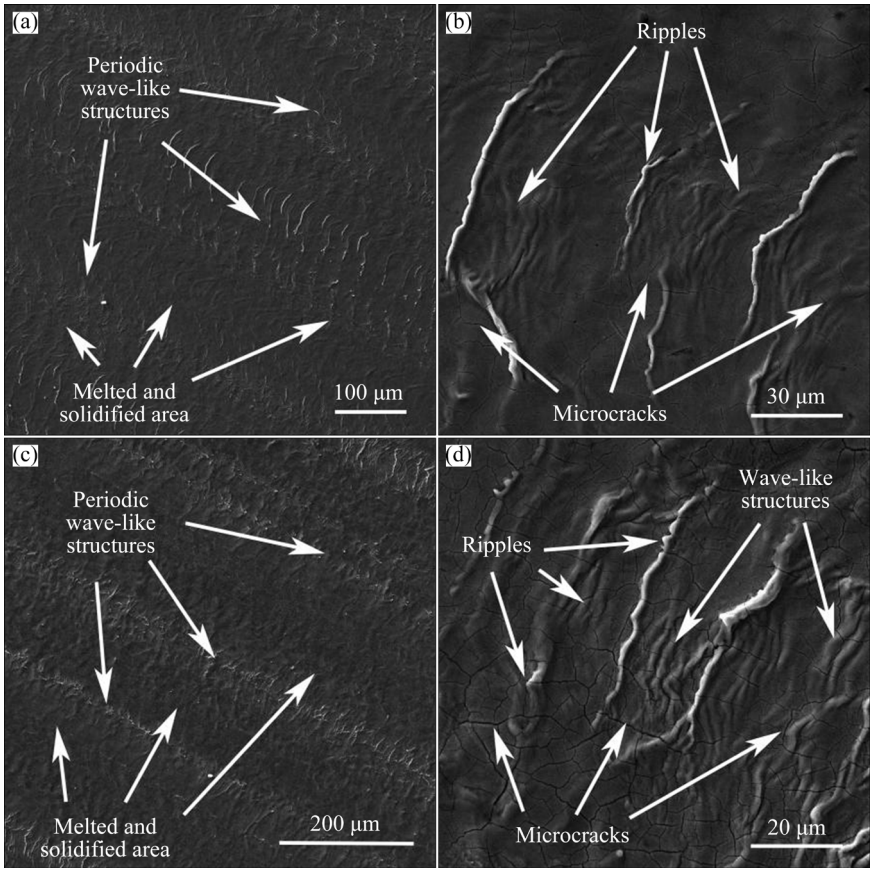

Fig. 2 FE-SEM micrographs of Ti−45Nb alloy surface after laser surface scanning with irradiation energies of 5 mJ (a, b) and 15 mJ (c, d)

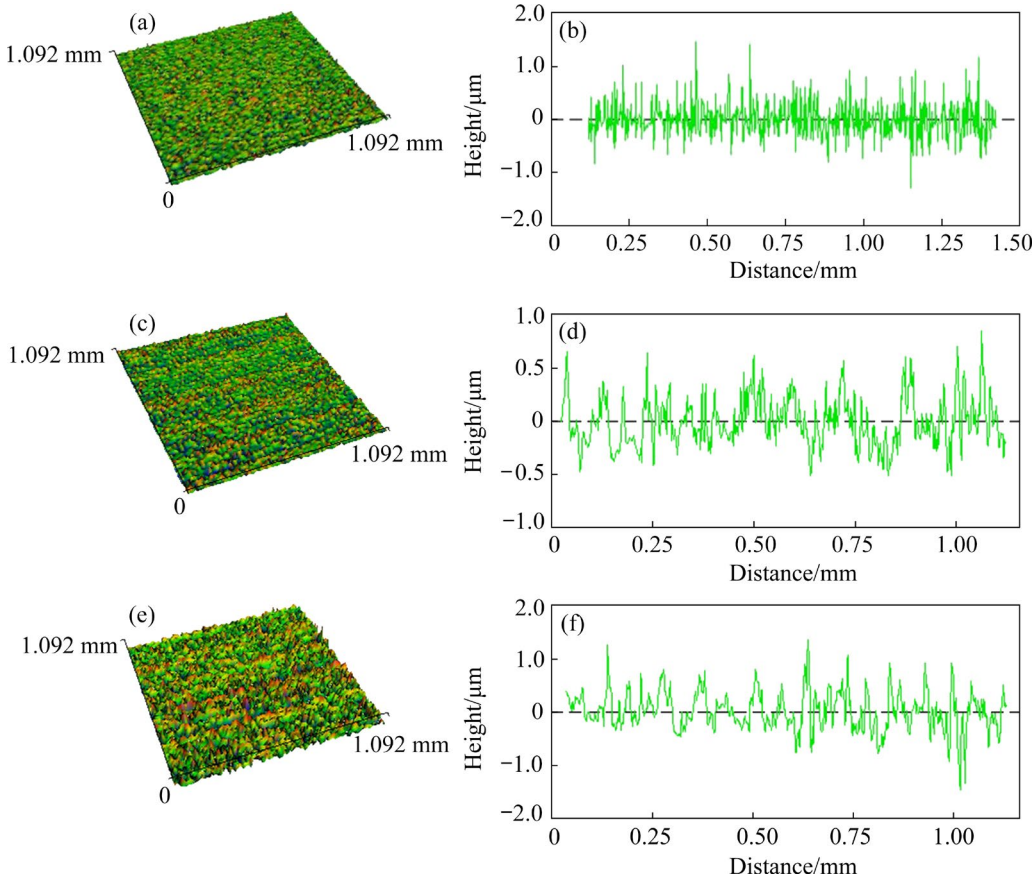

Fig. 3 3D (a, c, e) and linear (b, d, f) surface profiles obtained by profilometric analysis of Ti−45Nb alloy in as-received condition (a, b), and after laser irradiation with irradiation energies of 5 mJ (c, d) and 15 mJ (e, f)

pulse energy the surface roughness also increased. This is a result of the movement within the pool of melted material due to the tendency of hotter and, therefore, less dense material to spread, and the subsequent material rapid cooling which consequently resulted in more pronounced material surface modifications induced by the usage of laser beam TEM_{00} mode [14,16,17].

The initial surface roughness of the as-received Ti−45Nb alloy sample was determined as 0.186 μm and the surface was very smooth. At this roughness value, the maximal height of material was in the range from −1.25 to 1 μm (Fig. 3(b)). As shown in Fig. 3, the laser treatment generated a rougher surface compared to the untreated sample depending on the laser ablation and irradiation breakthrough degree. Figure 3 showed that application of the laser pulse energy of 5 mJ did not significantly influence the overall surface roughness of the sample since low laser energy showed a low impact on the surface feature formation [16]. On the other hand, the laser-treated sample subjected to a laser pulse energy of 15 mJ showed a different trend (Fig. 3). An increase in energy led to an increase in the sample surface roughness (0.280 μm). The height of the ejected material for the samples laser-treated with 5 and 15 mJ was approximately 0.80 and 1.4 μm, respectively, while the depth of material during laser irradiation breakthrough was approximately 0.50 and 1.35 μm, respectively (Figs. 3(d, f)). This is in accordance with the study of XU et al [45] who focused on the surface morphology, roughness, and laser-induced defects on the femtosecond treated material surface. Their results showed that the laser-irradiated structures included the appearance of melted zone, nanofibers, and laser-induced periodic surface structures. Moreover, laser-induced periodic surface structures were oriented parallel to the laser beam polarization direction and, as temperature increased during the laser irradiation, re-melting and rapid solidification of the material caused fracture at the melted and non-melted material interface since the melted material was ejected backward to the laser scanning direction [45].

The analysis of the alloy surface after interaction with the laser beam revealed that the absorbed irradiation energy not only induced morphological alterations but also resulted in surface chemical composition changes. The obtained EDS results showed that, when the Ti and Nb were still present in similar proportions on the material surface before and after laser treatment, the alloy surface laser scanning influenced a significant increase of the oxygen content in the irradiated area (Table 1). Moreover, an increase in laser pulse energy from 5 to 15 mJ led to an increase of the oxygen content for more than 30% in the analyzed irradiated areas due to the stimulated oxidation process on the material surface. This was expected due to the high affinity of Ti toward oxygen. The formation of such a surface oxide scale is favorable to the enhancement of the surface topography, bioactivity, corrosion resistance in the biological environment, and biocompatibility [6,26,46]. The obtained results (Fig. 1(b) and Table 1) indicate the formation of a stable, thin layer on the alloy surface composed of Ti- and Nb-oxides, which is in accordance with data in the literature [20,23]. The presence of such a surface oxide layer is favorable to the implant material biocompatibility and limits the alloying ions release into the surrounding living tissues [25,53−55]. The additional formation of oxides on the Ti−45Nb alloy surface during the laser treatment can modify the corrosion protection characteristics of the spontaneously-formed oxides and show a positive effect on the overall alloy corrosion resistance. Since the newly-formed oxide layer consists of (Ti,Nb)O oxides, it can be assumed that the presence of these oxides with a higher protective capacity will improve not only the alloy corrosion behavior but also the implant material−cells interactions and in that way contribute to the successful implantation process [25,26].

When a Ti−Nb alloy is exposed to oxygen, due to its direct contact with air, the surface layer, consisting of the alloying element oxides, is formed [20,23,54]. If this newly-formed layer is steady, it may serve as a protective layer for this material. The oxide layer growth and increase of its thickness can induce the improved cell adhesion and proliferation, osseointegration, as well as alloy corrosion resistance in the bio-environment [56−58]. Also, the observed increase in the oxide layer thickness with an increase in the laser output energy is coincidental with an increase in the alloy surface roughness, which can induce the improved alloy biointegration and bioactivity [44,46].

Table 1 Average oxygen contents on laser-irradiated Ti−45Nb alloy surface depending on laser output energy

Alloy	Surface oxygen content/wt.%	Standard deviation (SD)/%
Laser-irradiated with 5 mJ	14.51	0.65
Laser-irradiated with 15 mJ	21.39	0.71

3.3 Electrochemical behavior

To determine the effect of laser surface scanning modification on the corrosion resistance of the Ti−45Nb alloy, the alloy electrochemical behavior was evaluated in simulated physiological conditions.

The potentiodynamic polarization curves of the alloy in as-received and laser-treated conditions, obtained during testing in Ringer's solution at the human body temperature, are presented in Fig. 4. From the presented curves it can be observed that the Ti−45Nb alloy passivates when exposed to the investigation conditions irrespective of the laser surface treatment. However, its anodic polarization behavior differs as the alloy surface characteristics differ and only one passivating zone (denoted as I in Fig. 4) for the alloy in as-received condition and two passivating zones (denoted as I and II in Fig. 4) for the alloy in laser-treated condition can be distinguished in the anodic branch of alloy polarization curves.

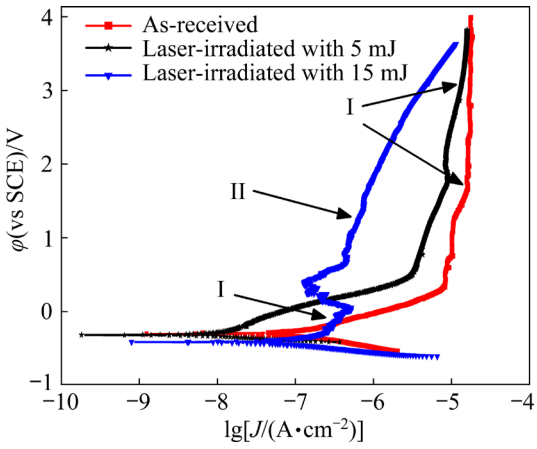

Fig. 4 Potentiodynamic polarization curves of as-received and laser-irradiated Ti−45Nb alloys obtained in naturally aerated Ringer's solution at 37 °C

After the immersion of alloy samples in the SBF solution, the spontaneous formation of surface oxide films was initiated until the stabilization of open circuit potential (φ_{OCP}) value was reached. These spontaneously formed films thicken with an increase of the anodic current density at potential from the corrosion potential (φ_{corr}) value to approximately 0.3 V (vs SCE) for the alloy samples in as-received condition, and to 0.5 V (vs SCE) and −0.4 V (vs SCE) for the alloy samples laser-treated with 5 and 15 mJ output energy, respectively.

For the laser-untreated alloy sample at the potential of 0.3 V (vs SCE) the current density value stabilizes almost completely, and with further increase of the potential value up to 4 V (vs SCE), it changes insignificantly from 7.94×10^{-6} to 1.96×10^{-5} A/cm^2, indicating the alloy surface passivation during the exposure to corrosive environment (passivating zone marked as I in Fig. 4) with the formation of stable oxide surface film [48,54]. The observed passivating region covers a wide potential range of 3.7 V (vs SCE) and indicates efficient passivation of the material surface by the formed oxide layer [24,30,58].

However, in the potentiodynamic polarization curve of the alloy sample laser-irradiated with 5 mJ, the presence of two distinct passivating regions can be distinguished. The primary passivating zone, marked as I in Fig. 4, covers the potential range from 0.5 to 1.7 V (vs SCE) where only a slight increase of the anodic current density value can be observed until it was stabilized at 7.08×10^{-5} A/cm^2. Further increase of the potential value to 1.85 V (vs SCE) is accompanied by an increase of the current density till the appearance of anodic peak at ~8×10^{-5} A/cm^2, which suggests a slight change in the surface oxide scale composition or appearance of some irregularities in the external oxide scale that covers the laser-treated alloy surface [48,58]. Above 1.85 V (vs SCE) the anodic current density only slightly decreases till the value of ~7.5×10^{-5} A/cm^2 is reached and completely stabilized, indicating the presence of a secondary passivating zone in the potential range from 2 to 4 V (vs SCE). This secondary passivating region, which is marked as II in Fig. 4, is the characteristic of the surface repassivation process and formation of the compact oxide scale that covers the entire alloy surface. The current density values in the passive regions are smaller than the ones recorded for the as-received alloy, indicating its greater stability.

On the other hand, the anodic polarization behavior of the alloy laser-irradiated with 15 mJ output energy significantly differs. Except for the presence of two distinct passivating regions, the active-passive nose in the potentiodynamic polarization curve can be observed. Namely, the first passivating region, denoted as I in Fig. 4, is observed in the potential range from −0.4 to 0 V (vs SCE) where the current density value modestly increases from 2.51×10^{-7} to 6.31×10^{-7} A/cm^2. With further increase of the potential value, the active−passive nose appears due to the occurrence of a diffusion process during which the complex oxide is formed on the alloy surface. Namely, with an increase of the potential value from 0 to 0.37 V (vs SCE) the current density value decreases until it reaches 1.26×10^{-7} A/cm^2 where the active-to-passive transition occurs, and the current density value shifts toward more positive values. Finally, at 0.7 V (vs SCE) the current density value stabilizes at 5.01×10^{-7} A/cm^2, indicating the formation of a barrier layer on the alloy surface, marking the second passivating zone, denoted as II in Fig. 4. However, the current density values are not constant in this region until the end of the polarization measurements at 4 V (vs SCE) due to the thickening of the formed complex oxide layer. Still, they are over an order of magnitude smaller as compared to values for other two samples, pointing to the formation of a stable layer.

The appearance of the second passivation region in the anodic branch of potentiodynamic polarization curves of the laser-irradiated samples suggests that both sample groups (irradiated with 5 and 15 mJ) showed a high corrosion resistance and a high passivation ability in the human body conditions [31,32,56].

The influence of the laser surface scanning treatment on the corrosion behavior of the Ti−45Nb alloy can also be analyzed through the obtained corrosion potential, φ_{corr}, and corrosion current density, J_{corr}. Values for the alloys before and after laser surface treatment are given in Table 2.

Low values of the corrosion current density attained for the untreated and laser-treated alloy samples (lower than 10^{-8} A/cm^2) indicate their

Table 2 Corrosion potentials (φ_{corr}) and corrosion current densities (J_{corr}) of Ti−45Nb alloys before and after laser surface scanning treatment obtained during electrochemical tests in naturally aerated Ringer's solution at 37 °C

Alloy	φ_{corr}(vs SCE)/V	J_{corr}/(10^{-8} A·cm^{-2})
As-received	−0.305±0.016	2.84±0.03
Laser-irradiated with 5 mJ	−0.332±0.009	0.65±0.01
Laser-irradiated with 15 mJ	−0.422±0.017	2.77±0.04

exceptional stability against corrosion damage and high durability of the investigated alloy in a simulated bio-environment regardless of the obtained laser-induced surface modifications. From the potentiodynamic polarization curves shown in Fig. 4 and results presented in Table 2, it can be observed that the corrosion current density values are the lowest for the sample laser-treated with 5 mJ compared to the values obtained for the as-received alloy and the sample laser-treated with 15 mJ. The formation of the stable and compact surface oxide layer during the laser scanning treatments influenced an obvious improvement of the alloy corrosion resistance properties and better corrosive damage tolerance in simulated body conditions. This is especially pronounced for the alloy subjected to laser irradiation with 5 mJ of output energy. Namely, the alloy sample irradiated with 5 mJ showed the lowest J_{corr} value (0.65×10^{-8} A/cm^2), which is about 77% lower than the value of corrosion current density recorded for the laser untreated alloy (2.84×10^{-8} A/cm^2) and the alloy laser-irradiated with 15 mJ (2.77×10^{-8} A/cm^2). Greater J_{corr} value for the sample irradiated with 15 mJ than with 5 mJ is probably due to the appearance of more prominent microcracks observed in Fig. 2. It can be noted that the formation of the more stable protective surface oxide film caused a superior passive behavior in both laser-treated samples than in the case of the alloy in as-received condition. Furthermore, the observed better corrosion stability of the laser-treated alloy compared to the untreated alloy shows that the corrosion behavior and resistance of the alloy are influenced by thickness of the formed oxide layer which, in turn, is affected by the surface laser scanning process.

In order to characterize the surface films and their stability, the electrochemical behavior of the Ti−45Nb alloys before and after laser treatment was additionally analyzed by conducting the EIS measurements in a simulated bio-environment. The obtained data are presented as the impedance spectra shown in Fig. 5 and electrochemical parameters given in Table 3.

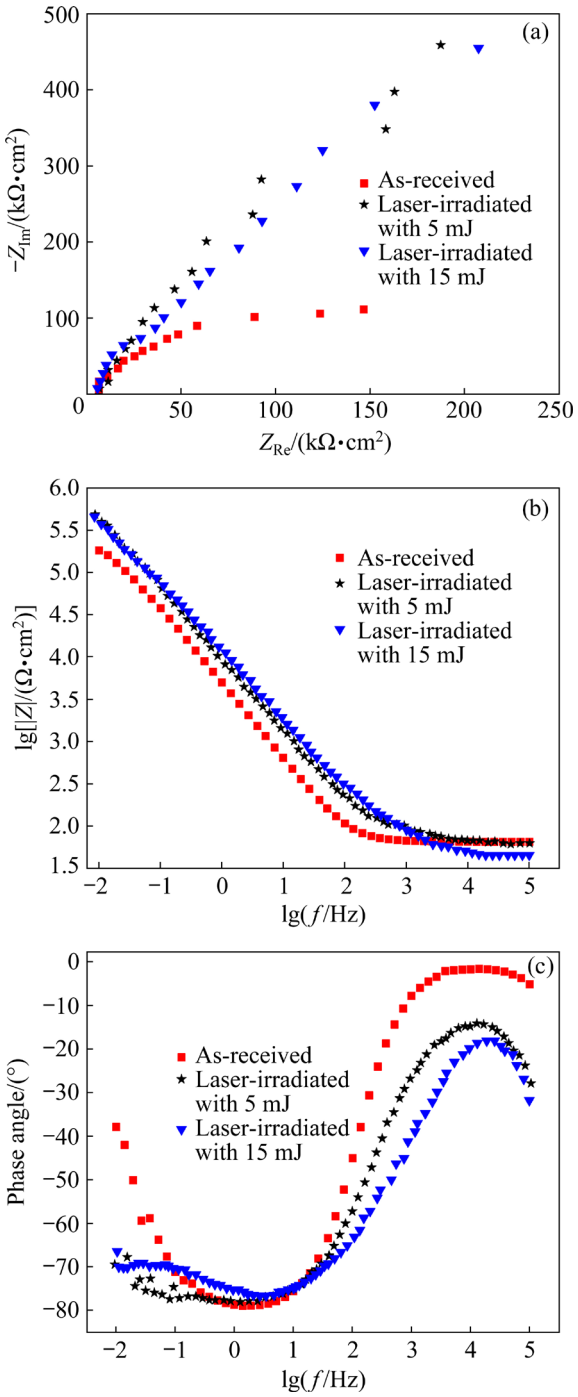

Fig. 5 EIS spectra of Ti−45Nb alloys before and after laser irradiation obtained in naturally aerated Ringer's solution at 37 °C: (a) Nyquist plot; (b) Bode plot (f represents frequency); (c) Bode phase angle plot

The analysis of the Nyquist plot given in Fig. 5(a) shows that even though a semicircle dependence of the real (Z_{Re}) and imaginary (Z_{Im}) components of the impedance is observed for all investigated samples, the overall impedance values are the lowest in the case of the alloy in as-received condition. This indicates that the protective surface films are formed on the Ti−45Nb alloy surface regardless of its surface laser treatment. However, the lowest overall impedance values and the more pronounced resistive response observed for the laser-untreated alloy sample reveal that the oxide films formed on its surface provide the lowest protection from corrosive degradation. Although the overall impedance values are similar in the case of both laser-treated samples, a somewhat greater value in the case of the alloy sample subjected to laser irradiation with 5 mJ of output energy suggests better protective properties of the oxide film formed on its surface.

In addition, based on the Bode diagrams that show the dependence of impedance modulus ($|Z|$) and phase angle (θ) on frequency (f) presented in Figs. 5(b, c), one can observe two characteristic frequency regions that are typical for the formation of two-layered oxide film on the surface of alloy samples in both untreated and laser-treated conditions. The presence of these two distinct frequency regions, i.e. two relaxation time constants, suggests that the alloy surface, regardless of its additional laser irradiation treatment, is covered by the surface film with a bi-modal structure composed of the inner barrier layer and the outer porous layer [57]. The appearance of the specific linear region over the wide frequency range in the Bode modulus plot given in Fig. 5(c) suggests the highly capacitive behavior of the barrier layers formed on the surface of all investigated samples. The observed high impedance values in the range from 10^5 to $10^6\ \Omega\cdot cm^2$ in the low-frequency region suggest that all investigated samples, regardless of their additional laser surface treatment, show good resistance to corrosion in Ringer's solution at 37 °C (Fig. 5(b)) [48,57]. However, the positive influence of surface laser treatment on the Ti−45Nb alloy corrosion resistance is indicated by the presence of a much broader phase angle peak at intermediate frequencies for the alloy samples subjected to laser irradiation regardless of the applied laser output energy (Fig. 5(c)). Furthermore, for the alloy sample in as-received condition in the high-frequency region, the low impedance values of $\sim 10^2\ \Omega\cdot cm^2$ (Fig. 5(b)) and phase angles close to 0°, compared to phase angles of −15° and −20° observed for the alloy samples laser-treated with 5 and 15 mJ (Fig. 5(c)), respectively, suggest the formation of thicker outer porous layer [30,53−55]. On the other hand, phase angles of −80° observed at intermediate frequencies for all test samples indicate the formation of a stable inner barrier layer regardless of the alloy surface irradiation treatment, while low phase angles (in the range from −65° to −80°) observed in the low-frequency region for the laser-treated samples imply that the additional laser surface modification induced the formation of a more stable barrier layer.

Fitting of the obtained EIS data was conducted by applying the equivalent electrical circuit (EEC) model with two relaxation time constants presented in Fig. 6 that corresponds to a two-layered passive surface film with outer porous (p) and inner barrier (b) layers [25,48]. The resistance of electrolyte, outer porous layer, and inner barrier layer in this EEC model are represented by components marked as R_Ω, R_p, and R_b, respectively. To describe the capacitive behavior of the outer porous and inner barrier layers formed on the alloy surface, the constant phase elements (CPE) marked as CPE_p and CPE_b, respectively, are used instead of the full capacitor (C) elements to take into account their discrepancy from the ideal capacitive behavior. The accuracy and quality of conducted data fitting are evaluated by using the "Goodness of fit" parameter where the obtained value lower than 10^{-3} for this parameter (Table 3) indicated good fitting of the EIS data with the selected EEC model.

According to the electrochemical parameters presented in Table 3, the resistance of outer porous layer, R_p, and the resistance of inner barrier layer,

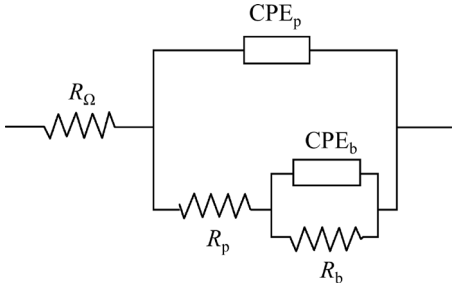

Fig. 6 Schematic representation of EEC model used for EIS data fitting

Table 3 Electrochemical parameters of Ti−45Nb alloy before and after laser surface scanning treatment obtained in naturally aerated Ringer's solution at 37 °C

Alloy	R_Ω/ Ω	Outer porous layer			Inner barrier layer			Goodness of fit
		R_p/ (Ω·cm^2)	CPE$_p$		R_b/ (Ω·cm^2)	CPE$_b$		
			Y_0/ (10^{-6} Ω^{-1}·cm^{-2}· s^n)	n		Y_0/ (10^{-6} Ω^{-1}·cm^{-2}· s^n)	n	
As-received	65.0	39.2	21.8	0.96	0.27×10^6	17.5	0.79	203.6×10^{-6}
Laser-irradiated with 5 mJ	42.2	130	4.37	0.77	3.09×10^6	14.8	0.88	0.44×10^{-3}
Laser-irradiated with 15 mJ	44.2	144	8.24	0.74	3.02×10^6	9.01	0.87	1.28×10^{-3}

R_b, which are formed on the surface of alloy in as-received condition are approximately 78% and 90% lower than those in the case of alloy with laser-treated surface, respectively. This indicates that the laser-irradiation treatment significantly increases the protective properties of the externally formed scales. Moreover, data presented in Table 3 shows that the inner barrier layer plays a decisive role in the improvement of alloy corrosion stability, especially after the laser scanning treatment, since the resistance of inner barrier layers is 4 orders of magnitude higher than that of outer porous layers for the alloy in all testing conditions.

Moreover, from the obtained fitted data presented in Table 3, the estimation of the capacitance (C) can be undertaken using the relation $C=[Y_0R^{-(n-1)}]^{1/n}$, where Y_0 represents the general admittance function, while n is the CPE power exponent with a value of $0\leq n\leq 1$ that indicates discrepancy from pure capacitive behavior (when n is equal to 0, the CPE element acts as a resistor; when n equals 1, the CPE element acts as a pure capacitor) [25]. The estimated barrier layer capacitance (C_b) for the alloy in as-received condition and after laser-irradiation with 5 and 15 mJ is 2.89×10^{-6}, 5.21×10^{-6}, and 2.78×10^{-6} s/(Ω·cm^2), respectively. On the other hand, the obtained porous layer capacitance (C_p) of the alloy in as-received condition and after laser-irradiation with 5 and 15 mJ is 16.59×10^{-6}, 0.34×10^{-6} and 0.51×10^{-6} s/(Ω·cm^2), respectively.

Having this in mind and using the relation $d=\varepsilon\varepsilon_0A/C$ [25], where ε, ε_0, and A are the oxide dielectric constant, vacuum dielectric permittivity, and effective surface area, respectively, the thickness of the formed inner barrier layer, d_b, can be determined and it is apparent that the thickness of barrier layer formed on the surface of as-received alloy, $d_{b(as\text{-}received)}$, is two times higher than that in the case of the alloy laser-treated with 5 mJ and almost the same as that in the case of the alloy laser-treated with 15 mJ, i.e. $d_{b(as\text{-}received)}\approx2d_{b(5\ mJ)}$, and $d_{b(as\text{-}received)}\approx d_{b(15\ mJ)}$. On the other hand, thickness of the formed outer porous layer, d_p, is significantly smaller on the surface of as-received alloy sample, i.e. $d_{p(as\text{-}received)}\approx0.02d_{p(5\ mJ)}$, and $d_{p(as\text{-}received)}\approx 0.03d_{p(15\ mJ)}$. These results indicate that in the case of the laser-untreated alloy during the corrosion in bio-environmental conditions, thicker barrier layer is formed; while in the case of the laser-treated alloy samples, thicker porous layer in the external scale is formed.

Since the resistance to corrosion degradation of the alloy laser-irradiated with 5 mJ is the highest, even though the thinnest barrier and the thickest porous layers are observed on its surface, the results of this study confirm the previously reported findings that the corrosion resistance of the titanium alloys is governed by the formation of a denser, more stable and compact barrier layer, while the thickness of porous layer mainly affects the material osseointegration properties [30,48]. Hence, this compact inner layer formed on the surface of alloy laser treated with 5 mJ, although thin, provides an effective barrier to electrolyte entry, resulting in the increased corrosion stability of the alloy, while much thicker porous films obtained on the surface of laser-irradiated alloy samples should provide their improved biocompatible response in the bio-environmental conditions.

Findings of the present study are in agreement with the research of JEONG et al [59] who concluded that an increase in corrosion resistance of the Ti−35Nb−10Zr alloy was enabled by using the laser surface texturing technique since the formation of thicker, more protective, and more

stable passivating surface scales was boosted during the alloy laser processing. This increase is enabled due to the enhanced reaction of oxygen with the molten material accumulated in the laser-modified area during the initial laser irradiation stages [40,53,55,58]. On the other hand, JEONG et al [60] showed that the oxide layers, present on the alloy surface after laser surface modification, resulted in the enhancement of cell proliferation, with presumably improved biocompatibility, and extensive spreading of the cells on the surfaces.

To investigate the correlation between the formation of outer porous scales and the alloy biocompatible properties, the in vitro testing methods were used.

3.4 Biological response

3.4.1 Cytotoxicity

The Ti−45Nb alloy before and after laser surface scanning was subjected to cytotoxicity testing to evaluate its biocompatibility in the simulated human body conditions. The MTT and DET methods were used to determine the viability of MRC-5 cells in contact with the investigated alloy and obtained results are presented in Table 4.

As shown in Table 4, during the MTT test the lowest average viability value of 91.23% was attained for MRC-5 cells in contact with the as-received alloy samples, while the MRC-5 cells in contact with the alloy laser-irradiated with 5 and 15 mJ output energy showed higher average viability of 94.89% and 115.37%, respectively. Based on these results it can be concluded that the investigated alloy showed excellent biocompatible properties regardless of its additional laser surface treatment. However, the viability of cells in contact with the untreated alloy surface was the lowest, indicating that laser surface scanning is the efficient method for the improvement of the biocompatible properties of the alloy. Based on the results attained after 48 h of cells exposure it was shown that the highest cell survival rate was achieved when the cells were in contact with the alloy samples irradiated with 15 mJ followed by the alloy samples irradiated with 5 mJ of output energy.

Table 4 Average cell viability of different samples obtained by MTT and DET assays after 48 h

Tested sample	Cell viability/%	
	MTT assay	DET assay
Control	100	100
As-received Ti−45Nb alloy	91.23	79.45
Ti−45Nb alloy laser-irradiated with 5 mJ	94.89	80.83
Ti−45Nb alloy laser-irradiated with 15 mJ	115.37	83.42

The DET test results, presented in Table 4, showed that the average viability of MRC-5 cells was the lowest in contact with the as-received alloy after 48 h of testing (79.45%). Higher average cell viability of 80.83% was observed in contact with the sample subjected to irradiation with 5 mJ of output energy, while the highest mean cell viability was recorded in the case of sample laser-irradiated with 15 mJ (83.42%). Based on the results of MTT and DET tests, it can be concluded that the highest degree of surviving cells was observed for a sample that was modified by laser scanning with energy of 15 mJ, indicating its highest cytocompatibility. In general, the investigated Ti−45Nb alloys in all conditions, untreated and laser-treated, show exceptional properties since all tested samples were proved to be not cytotoxic, and the alloy biocompatibility was estimated to be excellent.

3.4.2 Morphology of live cells

The morphology of MRC-5 cells in contact with the surface of Ti−45Nb alloy samples, before and after laser surface modification, is presented in Fig. 7. The shape of the cells observed on the unmodified and modified alloy samples indicates their excellent spread over the material surface. The observed cells showed a high tendency to integrate and create a continuous cell layer on the alloy surface, which is a confirmation of their good metabolic activity [44].

From the FE-SEM micrographs presented in Fig. 7, it was evident that the surface properties generated by the laser irradiation were more favorable to the fibroblast cells attachment. Furthermore, the cells present on the laser-treated surfaces showed good spreading through the formation of filopodia, indicating good cell adhesion.

Figures 7(a, b) also showed that the fibroblast cells present on the surface of alloy in as-received condition underwent initial spreading and the individual cells were observed to have 10−15 μm in length. As shown in Figs. 7(c, d), the laser surface scanning led to the formation of elongated

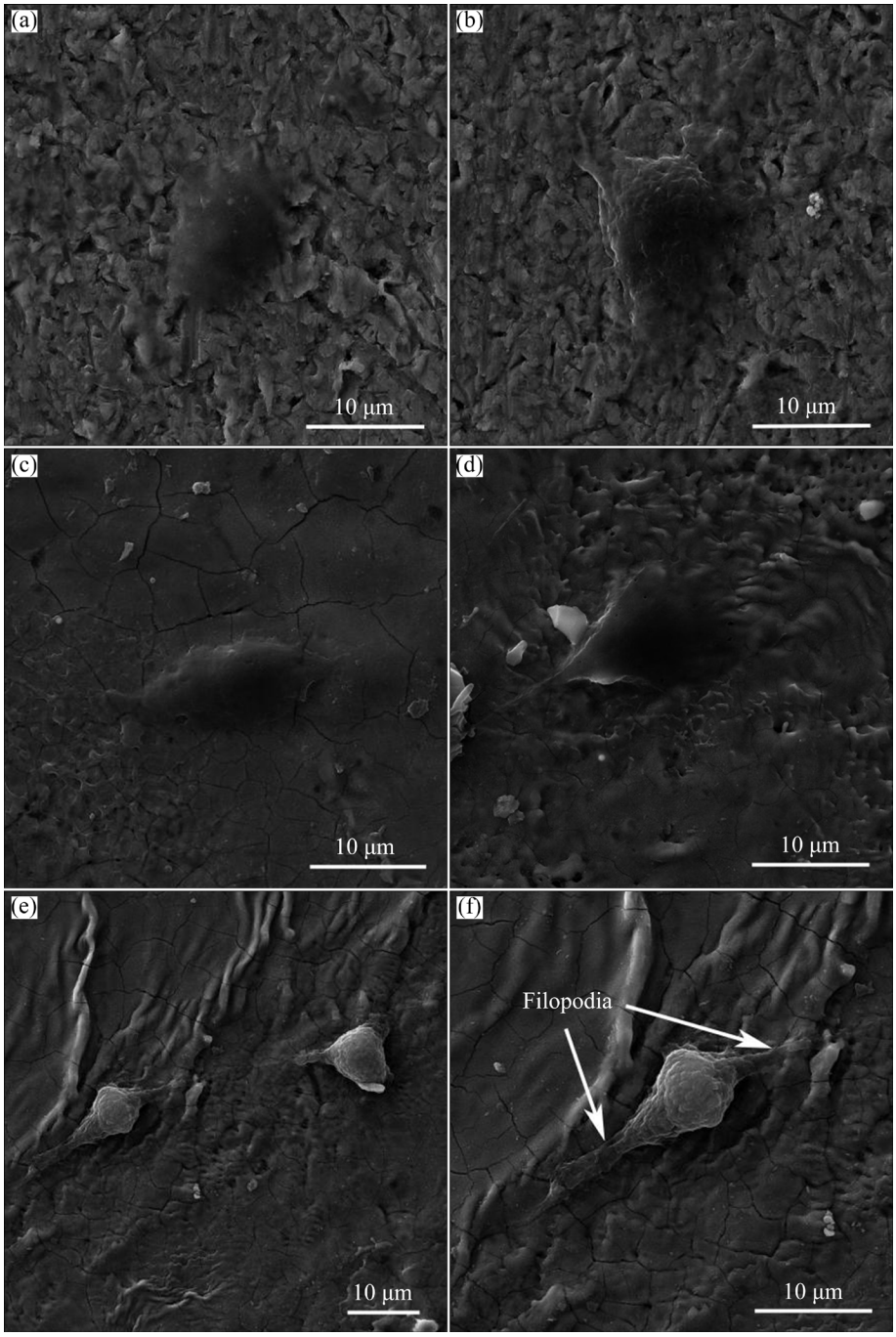

Fig. 7 FE-SEM micrographs of MRC-5 cells attached to surface of Ti−45Nb alloys: (a, b) As-received; (c, d) Laser-irradiated with 5 mJ output energy; (e, f) Laser-irradiated with 15 mJ output energy

fibroblast cells which spread to 20−30 μm in length. The fibroblast cells on the sample treated with higher energy of 15 mJ had spread completely over the irradiated area and formed pronounced cytoplasmic extensions (Figs. 7(e, f)). Short filopodia extend beyond every individual cell and elongate to a length of 2−5 μm, as presented in Fig. 7(f). The filopodia elongation direction implies the migration process direction [46]. The morphologies of these fibroblast cells display the final stage of cell attachment. In general, fibroblast cells in the irradiated area between two periodic scan lines spread better and achieve a more pronounced attachment to the surface than those at the edge of the laser-treated scan lines. Since the laser treatment caused diverse morphological alterations of the alloy surface as a result of the intensity distribution of the laser beam, it could be

concluded that fibroblast cell spreading and attachment were influenced by the level of the laser surface irradiation [38,44]. The above commented results confirm that the laser-treated surfaces represent a good cell growing environment without cytotoxic effect. Furthermore, the material surface examination did not reveal the presence of round cells without cytoplasmic extensions, which indicates excellent biocompatibility of all investigated samples [39,43].

3.4.3 Biocompatibility

On the other hand, when analyzing the biocompatibility of metallic implant materials, it should be taken into consideration that biocompatibility is influenced by a number of factors [33,34]. Two characteristics of the implant surface are proven to be the most important for its biocompatibility and osseointegration assessment: surface topography and chemical composition [38,44]. Compared to the smooth implant material surface, the controlled rough surface provides a larger surface area for integration with the surrounding tissues and allows the implant to grow into the tissues [38,45]. Previously published results indicate that higher roughness of the titanium-based implant surface improves the rate of its osseointegration [39,47]. Namely, MANJAIAH and LAUBSCHER [61] investigated the influence of surface modification on the thickness and composition of oxide layers formed on the surface of commercially pure titanium and its surface topography, and found that increasing the surface layer thickness up to 160 nm, and surface roughness from 16.3 to 37.2 nm had a positive effect on the material cytocompatibility. Moreover, JIAO et al [62] showed that the laser surface modification of biomaterials had a positive influence on their cytocompatibility by inducing more pronounced morphological features and the presence of metallic oxides in surface layers, as well as by enhancing surface roughness. This is also in agreement with the results of LIU et al [63], which show that porous and more developed surface provides more footholds for cell adhesion, leading to the firm cell adherence to the biomaterial surface and its implementation into the porous surface structure.

Furthermore, available research data show that laser irradiation of the metallic implant surface affects cell attachment and morphology through the formation of specific implant surface morphology with increased roughness that leads to an increased fibroblast cells elongation, better cells attachment to the modified implant surface, and their better bio-activity [37,39−42].

Since the material biocompatibility is very closely related to the cells behavior on the implant surface, such as cell attachment, spreading, and proliferation, an improvement of the biological response of biometallics leads to the better long-term stability of the surgically implanted medical aid [33,37,39,43,47]. Moreover, in addition to their increased roughness, surfaces with laser-induced damage features can induce diverse cell behavior, and particularly affect the direction of cells movement. As shown in Fig. 7, the laser-treated samples with rougher surfaces show a higher attachment rate of fibroblast cells compared with the smoother laser untreated surface, which is in good agreement with previous reports that the rougher biomaterial surface promotes better fibroblast-like cell attachment [43−45].

The implant material topography also significantly affects the adhesion and proliferation of human cells [38,61]. ZHAO et al [64] showed that the roughness of laser-treated surface of the Ti6Al4V alloy coated with Zr-oxides was significantly improved and that the presence of micro-grooves on the material surface in great merit influenced cell response by promoting cells to spread faster in the direction of grooves and achieve better cell adhesion and proliferation. Results of the present study are in good agreement with the above-mentioned findings and show significant improvement of the Ti−45Nb alloy biocompatible characteristics induced by the laser surface scanning treatment.

4 Conclusions

(1) Laser surface modification caused melting, solidification, and ablation of the Ti−45Nb alloy surface, and as a result, specific pattern lines with periodic wave-like structures and ripples were generated. More pronounced changes in the surface damage characteristics were recorded for the alloy laser-irradiated with pulse energy of 15 mJ.

(2) Laser scanning treatment altered the physicochemical properties of the native oxide layer, which in turn resulted in the enhancement of the corrosion resistance of Ti−45Nb alloy in the

simulated physiological conditions. The obtained J_{corr} values of 0.65×10^{-8} and 2.77×10^{-8} A/cm^2 for the samples laser-treated with pulse energy of 5 and 15 mJ, respectively, suggested a nobler passive behavior of the alloy subjected to the laser treatment with lower output energy.

(3) The bi-modal external oxide scale, composed of outer porous and inner barrier films, was formed on the alloy surface regardless of its additional laser-irradiation treatment. The compact inner layer formed on the surface of alloy laser-treated with 5 mJ, although thin, provides an effective barrier to electrolyte entry, resulting in the alloy increased corrosion stability, while much thicker porous films formed on the surface of laser-irradiated alloy samples provide their improved biocompatible response in the bio-environmental conditions.

(4) The results of the in vitro tests showed that all test groups showed biocompatibility without the appearance of unfavorable effects, indicating good cytocompatibility of the Ti−45Nb alloy irrespective of its additional surface laser treatment. However, laser treatment induced a considerable improvement in the response of fibroblast cells and resulted in the improved cell attachment and proliferation. Moreover, an increase in the laser pulse energy led to the surface roughness increase, which in turn led to the appearance of filopodia and the improved spreading of fibroblast cells.

(5) The results of the present study show that laser surface modification in great merit influences changes in the alloy surface morphology and chemistry, and is a suitable method for the improvement of Ti-based biometallic alloy corrosion resistance and biocompatibility.

CRediT authorship contribution statement

I. CVIJOVIĆ-ALAGIĆ: Conceptualization, Investigation, Methodology, Supervision, Writing – Original draft, Writing – Review & editing; **S. LAKETIĆ:** Conceptualization, Investigation, Writing – Original draft; **M. MOMČILOVIĆ:** Methodology, Investigation; **J. CIGANOVIĆ** and **Đ. VELJOVIĆ:** Investigation; **J. BAJAT** and **V. KOJIĆ:** Methodology, Investigation; **M. RAKIN:** Supervision.

Declaration of competing interest

The authors declare that they have no known competing financial interests or personal relationships that could have appeared to influence the work reported in this paper.

Acknowledgments

This work was financially supported by the Ministry of Science, Technological Development and Innovation of the Republic of Serbia (No. 451-03-47/2023-01/200017) and the PhD fellowship of Slađana LAKETIĆ. Authors would also like to acknowledge the help of Dr. Anton HOHENWARTER from the Department of Materials Science, Montanuniversitat Leoben, Austria, during the Ti−45Nb alloy microstructural analysis.

References

[1] KOIZUMI H, TAKEUCHI Y, IMAI H, KAWAI T, YONEYAMA T. Application of titanium and titanium alloys to fixed dental prostheses [J]. Journal of Prosthodontic Research, 2019, 63: 266−270.

[2] NNAMCHI P S, NJOKU R E, FASUBA O A. Alloy design and property evaluation of Ti−Mo−Nb−Sn alloy for biomedical applications [J]. Nigerian Journal of Technology, 2013, 32: 410−416.

[3] LI Y, YANG C, ZHAO H, QU S, LI X, LI Y. New developments of Ti-based alloys for biomedical applications [J]. Materials, 2014, 7: 1709−1800.

[4] DAVIDSON J A, MISHRA A K, KOVACS P, POGGIE R A. New surface-hardened, low-modulus, corrosion-resistant Ti−13Nb−13Zr alloy for total hip arthroplasty [J]. Bio-Medical Materials and Engineering, 1994, 4: 231−243.

[5] NOURI A, CHEN X B, HODGSON P D, WEN C E. Preparation and characterization of new titanium based alloys for orthopedic and dental applications [J]. Advanced Materials Research, 2007, 15/16/17: 71−76.

[6] YAMAZOE J, NAKAGAWA M, MATONO Y, TAKEUCHI A. The development of Ti alloys for dental implant with high corrosion resistance and mechanical strength [J]. Dental Materials Journal, 2007, 26: 260−267.

[7] CHEN L Y, CUI Y W, ZHANG L C. Recent development in beta titanium alloys for biomedical applications [J]. Metals, 2020, 10: 1139.

[8] PRASHANTH K G, ZHURAVLEVA K, OKULOV I, CALIN M, ECKERT J, GEBERT A. Mechanical and corrosion behavior of new generation Ti−45Nb porous alloys implant devices [J]. Technologies, 2016, 4: 33.

[9] CHEN Q, THOUAS G A. Metallic implant biomaterials [J]. Materials Science and Engineering: R: Reports, 2015, 87: 1−57.

[10] LIU X, CHU P K, DING C. Surface modification of titanium, titanium alloys, and related materials for biomedical applications [J]. Materials Science and Engineering R, Reports, 2004, 47: 49−121.

[11] NOURI A, WEN C. Introduction to surface coating and modification for metallic biomaterials [C]//Surface Coating and Modification of Metallic Biomaterials. Cambridge, UK: Elsevier, 2015: 3−60.

[12] HUSSEIN M, ADESINA A Y, KUMAR M, AZEEM M, SOROUR A, AL-AQEELI N. Improvement of in vitro corrosion, wear, and mechanical properties of newly developed Ti alloy by thermal treatment for dental applications [J]. Transactions of Nonferrous Metals Society of China, 2021, 31: 952−966.

[13] BROWN M S, ARNOLD C B. Fundamentals of laser-material interaction and application to multiscale surface modification [C]//Laser Precision Microfabrication. New York, USA: Springer, 2010: 91−120.

[14] MOMČILOVIĆ M D. Interaction of impulse TEA CO_2 laser radiation with copper target: Spectroscopy of plasma and morhological effects [D]. Belgrade: University of Belgrade, 2014.

[15] CARPENE E, HÖCHE D, SCHAAF P. Fundamentals of laser-material interactions [C]//Laser Processing of Materials: Fundamentals, Applications and Developments. Berlin: Springer, 2010: 21−47.

[16] LI X, GUAN Y. Theoretical fundamentals of short pulse laser−metal interaction: A review [J]. Nanotechnology and Precision Engineering, 2020, 3: 105−125.

[17] CIGANOVIĆ J V. Action of pulsed lasers on titanium target: Surface effects [D]. Belgrade: University of Belgrade, 2020.

[18] PATRASCU I, VASILESCU E, GATIN E, CARA-ILICI R R. Corrosion of biomaterials used in dental reconstruction dentistry [C]//Developments in Corrosion Protection. London: InTech, 2014: 633−658.

[19] POPOOLA A, OLORUNNIWO O, IGE O. Corrosion resistance through the application of anti-corrosion coatings [C]//Developments in Corrosion Protection. London: IntechOpen, 2014: 243−270.

[20] NASCIMENTO J P L, FERREIRA M O A, GELAMO R V, SCARMINIO J, STEFFEN T T, PEREIRA SILVA B, AOKI I V, SANTOS A G Jr, CASTRO V V, FRAGA MALFATTI C, MORETO J A. Enhancing the corrosion protection of Ti−6Al−4V alloy through reactive sputtering niobium oxide thin films [J]. Surface and Coatings Technology, 2021, 428: 127854.

[21] AFZALI P, GHOMASHCHI R, OSKOUEI R H. On the corrosion behaviour of low modulus titanium alloys for medical implant applications: A review [J]. Metals, 2019, 9: 878.

[22] GONZALEZ J E G, MIRZA-ROSCA J C. Study of the corrosion behavior of titanium and some of its alloys for biomedical and dental implant applications [J]. Journal of Electroanalytical Chemistry, 1999, 471: 109−115.

[23] GUTIERREZ A, LOPEZ M F, JIMENEZ J A, MORANT C, PASZTI F, CLIMENT A. Surface characterization of the oxide layer grown on Ti−Nb−Zr and Ti−Nb−Al alloys [J]. Surface and Interface Analysis, 2004, 36: 977−980.

[24] KHAN M A, WILLIAMS R L, WILLIAMS D F. The corrosion behaviour of Ti−6Al−4V, Ti−6Al−7Nb and Ti−13Nb−13Zr in protein solutions [J]. Biomaterials, 1999, 20: 631−637.

[25] CVIJOVIĆ-ALAGIĆ I, CVIJOVIĆ Z, BAJAT J, RAKIN M. Composition and processing effects on the electrochemical characteristics of biomedical titanium alloys [J]. Corrosion Science, 2014, 83: 245−254.

[26] DIMIĆ I, CVIJOVIĆ-ALAGIĆ I, HOHENWARTER A, PIPPAN R, KOJIĆ V, BAJAT J, RAKIN M. Electrochemical and biocompatibility examinations of high-pressure torsion processed titanium and Ti−13Nb−13Zr alloy [J]. Journal of Biomedical Materials Research, 2018, 106: 1097−1107.

[27] SITI NUR HAZWANI M R, LIM L X, LOCKMAN Z, ZUHAILAWATI H. Fabrication of titanium-based alloys with bioactive surface oxide layer as biomedical implants: Opportunity and challenges [J]. Transactions of Nonferrous Metals Society of China, 2022, 32: 1−44.

[28] WANG J, XIAO W, REN L, FU Y, MA C. The roles of oxygen content on microstructural transformation, mechanical properties and corrosion resistance of Ti−Nb-based biomedical alloys with different β stabilities [J]. Materials Characterization, 2021, 176: 111122.

[29] JIRKA I, VANDROVCOVÁ M, FRANK O, TOLDE Z, PLŠEK J, LUXBACHER T, BAČÁKOVÁ L, STARÝ V. On the role of Nb-related sites of an oxidized β-TiNb alloy surface in its interaction with osteoblast-like MG-63 cells [J]. Materials Science and Engineering C, 2013, 33: 1636−1645.

[30] YUE T M, CHEUNG T M, MAN H C. Effects of laser surface treatment on the corrosion properties of Ti−6Al−4V alloy in Hank's solution [J]. Journal of Materials Science Letters, 2000, 19: 205−208.

[31] MA C, PENG G, NIE L, LIU H, GUAN Y. Laser surface modification of Mg−Gd−Ca alloy for corrosion resistance and biocompatibility enhancement [J]. Applied Surface Science, 2018, 445: 211−216.

[32] SINGH R, MARTIN M, DAHOTRE N B. Influence of laser surface modification on corrosion behavior of stainless steel 316L and Ti−6Al−4V in simulated biofluid [J]. Surface Engineering, 2005, 21: 297−306.

[33] KASEMO B. Biological surface science [J]. Surface Science, 2002, 500: 656−677.

[34] GEPREEL M A H, NIINOMI M. Biocompatibility of Ti-alloys for long-term implantation [J]. Journal of the Mechanical Behavior of Biomedical Materials, 2013, 20: 407−415.

[35] SHAH A K, LAZATIN J, SINHA R K, LENNOX T, HICKOK N J, TUAN R S. Mechanism of BMP-2 stimulated adhesion of osteoblastic cells to titanium alloy [J]. Biology of the Cell, 1999, 91: 131−142.

[36] ZHAO D P, CHEN Y K, CHANG K K, EBEL T, LUTHRIGNER-FEYERABEND B J C, WILLUMEIT-RÖMER R, PYCZAK F. Surface topography and cytocompatibility of metal injection molded Ti−22Nb alloy as biomaterial [J]. Transactions of Nonferrous Metals Society of China, 2018, 28: 1342−1350.

[37] PARK J W, KIM Y J, PARK C H, LEE D H, KO Y G, JANG J H, LEE C S. Enhanced osteoblast response to an equal channel angular pressing-processed pure titanium substrate with microrough surface topography [J]. Acta Biomaterialia, 2009, 5: 3272−3280.

[38] LUZ A R, LIMA G G, SANTOS E, PEREIRA B L, SATO H H, LEPIENSKI C M, LIMA D B, LAURINDO C, GRANDINI C R, KUROMOTO N K. Tribo-mechanical properties and cellular viability of electrochemically treated Ti−10Nb and Ti−20Nb alloys [J]. Journal of Alloys and Compounds, 2019, 779: 129−139.

[39] LIN L, WANG H, NI M, RUI Y, CHENG T Y, CHENG C K, PAN X, LI G, LIN C. Enhanced osteointegration of medical titanium implant with surface modifications in micro/nanoscale structures [J]. Journal of Orthopaedic Translation, 2014, 2: 35−42.

[40] ZHAO X, ZHANG H, LIU H, LI S, LI W, WANG X. In vitro bio-tribological behaviour of textured nitride coating on selective laser melted Ti−6Al−4V alloy [J]. Surface and Coatings Technology, 2021, 409: 126904.

[41] LIU N, SUN Y, WANG H, LIANG C. Femtosecond laser-induced nanostructures on Fe−30Mn surfaces for biomedical applications [J]. Optics and Laser Technology, 2021, 139: 106986.

[42] LIU J, SONG Y, CHEN C, WANG X, LI H, ZHOU C, WANG J, GUO K, SUN J. Effect of scanning speed on the microstructure and mechanical behavior of 316L stainless steel fabricated by selective laser melting [J]. Materials & Design, 2020, 186: 108355.

[43] HOČEVAR M, ŠETINA BATIČ B, GODEC M, KONONENKO V, DROBNE D, GREGORČIČ P. The interaction between the osteosarcoma cell and stainless steel surface, modified by high-fluence, nanosecond laser pulses [J]. Surface and Coatings Technology, 2020, 394: 125878.

[44] DOU H, LIU H, XU S, CHEN Y, MIAO X, LÜ H, JIANG X. Influence of laser fluences and scan speeds on the morphologies and wetting properties of titanium alloy [J]. Optik, 2020, 224: 165443.

[45] XU S, DOU H, SUN K, YE Y, LI Z, WANG H, LIAO W, LIU H, MIAO X, YUAN X, JIANG X, ZU X. Scan speed and fluence effects in femtosecond laser induced micro/nano-structures on the surface of fused silica [J]. Journal of Non-Crystalline Solids, 2018, 492: 56−62.

[46] WANG Y, ZHANG J, LI K, HU J. Surface characterization and biocompatibility of isotropic microstructure prepared by UV laser [J]. Journal of Materials Science and Technology, 2021, 94: 136−146.

[47] KEDIA S, BONAGANI S K, MAJUMDAR A G, KAIN V, SUBRAMANIAN M, MAITI N, NILAYA J P. Nanosecond laser surface texturing of type 316L stainless steel for contact guidance of bone cells and superior corrosion resistance [J]. Colloid and Interface Science Communications, 2021, 42: 100419.

[48] CVIJOVIĆ-ALAGIĆ I, LAKETIĆ S, BAJAT J, HOHENWARTER A, RAKIN M. Grain refinement effect on the Ti−45Nb alloy electrochemical behavior in simulated physiological solution [J]. Surface and Coatings Technology, 2021, 423: 127609.

[49] LI W, ZHOU J, XU Y. Study of the in vitro cytotoxicity testing of medical devices (Review) [J]. Biomedical Reports, 2015, 3: 617−620.

[50] OZALTIN K, CHROMINSKI W, KULCZYK M, PANIGRAHI A, HORKY J, ZEHETBAUER M, LEWANDOWSKA M. Enhancement of mechanical properties of biocompatible Ti−45Nb alloy by hydrostatic extrusion [J]. Journal of Materials Science, 2014, 49: 6930−6936.

[51] CVIJOVIĆ-ALAGIĆ I, RAKIN M, LAKETIĆ S, ZAGORAC D. Microstructural study of Ti−45Nb alloy before and after HPT processing using experimental and ab initio data mining approach [J]. Materials Characterization, 2020, 169: 110635.

[52] LI S, CUI Z, ZHANG W, LI Y, LI L, GONG D. Biocompatibility of micro/nanostructures nitinol surface via nanosecond laser circularly scanning [J]. Material Letters, 2019, 255: 126591.

[53] CREMASCO A, OSORIO W R, FREIRE C M A, GARCIA A, CARAM R. Electrochemical corrosion behavior of a Ti−35Nb alloy for medical prostheses [J]. Electrochimica Acta, 2008, 53: 4867−4874.

[54] FOJT J, JOSKA L, MÁLEK J. Corrosion behaviour of porous Ti−39Nb alloy for biomedical applications [J]. Corrosion Science, 2013, 71: 78−83.

[55] LAVOS-VALERETO I C, WOLYNEC S, RAMIRES I, GUASTALDI A C, COSTA I. Electrochemical impedance spectroscopy characterization of passive film formed on implant Ti−6Al−7Nb alloy in Hank's solution [J]. Journal of Materials Science: Materials in Medicine, 2004, 15: 55−59.

[56] ASSIS S L, ROGERO S O, ANTUNES R A, PADILHA A F, COSTA I. A comparative study of the in vitro corrosion behavior and cytotoxicity of a superferritic stainless steel, a Ti−13Nb−13Zr alloy, and an austenitic stainless steel in hank's solution [J]. Journal of Biomedical Materials Research, 2005, 73: 109−116.

[57] ASSIS S L, COSTA I. Electrochemical evaluation of Ti−13Nb−13Zr, Ti−6Al−4V and Ti−6Al−7Nb alloys for biomedical application by long-term immersion tests [J]. Materials and Corrosion, 2007, 58: 329−333.

[58] ANIOŁEK K, ŁOSIEWICZ B, KUBISZTAL J, OSAK P, STRÓŻ A, BARYLSKI A, KAPTACZ S. Mechanical properties, corrosion resistance and bioactivity of oxide layers formed by isothermal oxidation of Ti−6Al−7Nb alloy [J]. Coatings, 2021, 11: 505.

[59] JEONG Y H, CHOE H C, BRANTLEY W A, SOHN I B. Hydroxyapatite thin film coatings on nanotube-formed Ti−35Nb−10Zr alloys after femtosecond laser texturing [J]. Surface and Coatings Technology, 2013, 217: 13−22.

[60] JEONG Y H, CHOE H C, BRANTLEY W A. Nanostructured thin film formation on femtosecond laser-textured Ti−35Nb−*x*Zr alloy for biomedical applications [J]. Thin Solid Films, 2011, 519: 4668−4675.

[61] MANJAIAH M, LAUBSCHER R F. Effect of anodizing on surface integrity of Grade 4 titanium for biomedical applications [J]. Surface and Coatings Technology, 2017, 310: 263−272.

[62] JIAO Y, BROUSSEAU E, NISHIO AYRE W, GAIT-CARR E, SHEN X, WANG X, BIGOT S, ZHU H, HE W. In vitro cytocompatibility of a Zr-based metallic glass modified by laser surface texturing for potential implant applications [J]. Applied Surface Science, 2021, 547: 149194.

[63] LIU G, LI Y, YAN M, FENG J, CAO J, LEI M, LIU Q, HU X, WANG W, LI X. Vacuum wetting of Ag/TA2 to develop a novel micron porous Ti with significant biocompatibility and antibacterial activity [J]. Journal of Materials Science & Technology, 2022, 116: 180−191.

[64] ZHAO Z, WAN Y, YU M, WANG H, CAI Y, LIU C, ZHANG D. Biocompability evaluation of micro textures coated with zinc oxide on Ti−6Al−4V treated by nanosecond laser [J]. Surface and Coatings Technology, 2021, 422: 127453.

激光处理对 Ti−45Nb 合金表面、腐蚀性能和生物相容性的影响

I. CVIJOVIĆ-ALAGIĆ[1], S. LAKETIĆ[1], M. MOMČILOVIĆ[1],
J. CIGANOVIĆ[1], Đ. VELJOVIĆ[2], J. BAJAT[2], V. KOJIĆ[3], M. RAKIN[2]

1. Vinča Institute of Nuclear Sciences-National Institute of the Republic of Serbia,
University of Belgrade, P.O. Box 522, 11001 Belgrade, Serbia;
2. Faculty of Technology and Metallurgy, University of Belgrade, Karnegijeva 4, 11120 Belgrade, Serbia;
3. Oncology Institute of Vojvodina, Faculty of Medicine,
University of Novi Sad, Put Dr Goldmana 4, 21204 Sremska Kamenica, Serbia

摘　要：研究 Ti−45Nb(质量分数，%)合金的性能及其潜在的生物医学应用。采用激光表面改性技术提高合金的生物学性能。经过激光处理后，合金表面形成了(Ti,Nb)O 氧化层和不同的形貌特征。评估了 Ti−45Nb 合金在模拟体液条件下的电化学行为，结果表明，无论是否进行激光表面改性处理，该合金都具有优异的耐腐蚀性。然而，激光处理后合金的耐腐性显著提高，经过 5 mJ 的激光处理后，合金的腐蚀电流密度从处理前的 2.84×10^{-8} A/cm 降低为 0.65×10^{-8} A/cm，这是由于快速形成了一种复杂且具有钝化作用的双模态表面氧化层。还研究了合金的细胞毒性以及 Ti−45Nb 合金激光表面改性对 MRC-5 细胞的活性、形态和增殖的影响。结果表明，Ti−45Nb 合金无细胞毒性。此外，细胞在激光处理后合金表面的活性和黏附性都有所提高。经 15 mJ 激光处理后，合金的平均细胞活性最高，为 115.37%。结果表明，激光表面改性可以成功用于显著提高合金细胞相容性。

关键词：Ti−45Nb 合金；激光表面扫描；电化学性能；生物相容性；细胞形态

(Edited by Wei-ping CHEN)